J. Membrane Biol. 81, 205–217 (1984)

The Journal of
Membrane Biology

Temperature Dependence of Single Channel Currents and the Peptide Libration Mechanism for Ion Transport through the Gramicidin A Transmembrane Channel

D.W. Urry, S. Alonso-Romanowski, C.M. Venkatachalam, R.J. Bradley† and R.D. Harris
Laboratory of Molecular Biophysics and †Neurosciences Program, University of Alabama in Birmingham, School of Medicine, Birmingham, Alabama 35294

Summary. A study of the temperature dependence of gramicidin A conductance of K^+ in diphytanoyllecithin/*n*-decane membranes shows the plot of ln (single channel conductance) as a function of reciprocal temperature to be nonlinear for the most probable set of conductance states. These results are considered in terms of a series of barriers, of the dynamics of channel conformation, *vis-a-vis* the peptide libration mechanism, and of the effect of lipid viscosity on side chain motions again as affecting the energetics of peptide libration.

Key Words gramicidin channel · temperature dependence · single channel current histograms · peptide libration mechanism · nonlinear Arrhenius plots · metastable states · dynamic channel

Introduction

The gramicidin A $\beta^{6,3}_{3,3}$ helical transmembrane channel [24, 25] has a diameter of about 4 Å. This is too small for hydrated ions to pass through and too large for adequate coordination of partially dehydrated ions. Because of this, in the initial proposal of the structure, a mechanism was described in which the carbonyl oxygens of the peptides rotated into the channel in order to decrease the channel radius from about 2 Å to the ionic radius of the permeant ion [25]. Shortly thereafter a more detailed discussion of the process referred to it as a peptide libration mechanism [24]. A peptide libration is a rocking motion or a torsional oscillation of the peptide moiety involving simultaneous changes in the ψ_i and ϕ_{i+1} torsion angles (*see* Fig. 1), i.e., compensating rotations about the αC_i-C'_i and N-αC_{i+1} single bonds such that the α-carbons exhibit minimal movement and the helical parameters are also minimally changed. Since the carbonyl oxygen carries a partial negative charge, a peptide libration moving oxygens into the channel introduces an attractive negative potential in the channel for cations and a repulsive positive potential for anions. By this mechanism the channel would be selectively permeable to cations. Now by invoking an energy dependence for the peptide libration that was proportional to the extent of libration from the relaxed channel conformation, a selectivity for cations is expected that would favor cations of larger ionic radii up to some limiting radius.

In the peptide libration mechanism, a conformation of the channel, subtly different from the most preferred conformation in the absence of anion, is required during transit of the ion through the channel. The mechanism itself does not specify whether the ion induces a metastable state of a detectable lifetime for the entire channel, whether the ion simply causes a local deformation, or whether the actual process is a combination of both, i.e., a metastable state with a discernible deformation at the instantaneous location of the cation. While a transient local deformation of some magnitude was described in the original discussions [24] in terms of a peristalsis with the constriction occurring at the location of the ion, more recent data and their analysis argue for the existence of metastable states.

Direct evidence for metastable states is found in the observation of a dispersity of single-channel currents commonly demonstrated by histograms of frequency of occurrence *versus* magnitude of single-channel conductances [2, 4, 14]. This multiplicity of single-channel conductance magnitudes initially could not be distinguished from the occurrence of combinations of structural analogs, such as gramicidin A, gramicidin B, gramicidin C, and other analogs and impurities, nor from the possibility of different end-to-end dimerizations [6], nor from the possibility of both left and right handed single and double stranded helices. It is now quite clear that such dispersity occurs with pure gramicidin A, whether synthetic or HPLC purified natural material [21], and that it occurs for the single

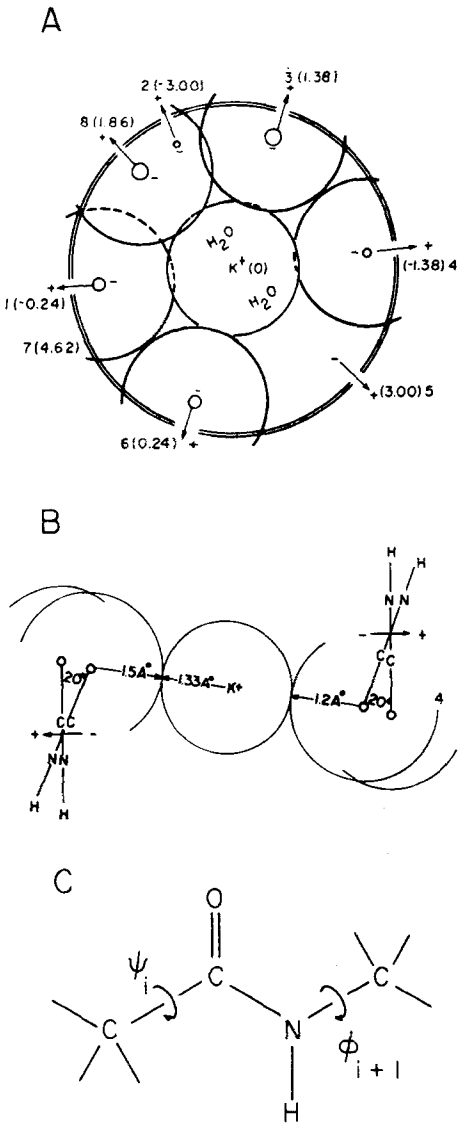

Fig. 1. The peptide libration mechanism. (*A*): Channel view depicting the carbonyl oxygens librated into the channel to make contact laterally with the bare potassium ion. (*B*): Transverse view showing the plane of the peptide to be librated about 20°. *A* and *B* have been reproduced from: Confirmation of Biological Molecules and Polymers (The Jerusalem Symposia on Quantum Chemistry and Biochemistry, V), Jerusalem, 1973, by the courtesy of The Israel Academy of Science and Humanities. (*C*): The peptide moiety spanning between α-carbons. A peptide libration is achieved by the coupled torsional motions involving ψ_i and the ϕ_{i+1} dihedral angles

stranded left-handed [33], head-to-head dimerized [2, 3, 24, 27, 35] $\beta^{6.3}_{3,3}$-helical gramicidin A channels, i.e., for the original proposed structure [24, 25].

The most explicit demonstration that the same basic structure can exhibit different magnitudes of single-channel currents comes from the work of Busath and Szabo [7]. They have observed that the most probable channel events exhibit symmetric current-voltage (*I-V*) curves while less probable channel events exhibit asymmetric *I-V* curves. Importantly, they have observed channels with symmetrical *I-V* curves which undergo transition to channels with asymmetric *I-V* curves. The same channel can exist in different conductance states and the transition can occur while continuously conducting, i.e., without turning off and coming back on. This requires time constants for metastable states of the order of seconds.

A second argument for metastability of channel states involves time constants of the order of microseconds. This derives from a comparison of nuclear magnetic resonance-derived binding constants and rate constants that successfully calculate sodium conductance [31, 32]. The sodium ion binding constants for the first and second ion differ by almost two orders of magnitude. Similar differences in binding constants between single and multiple occupancy have been found by Eisenman and coworkers and by Haydon and coworkers [11, 15]. With the twofold symmetry of the channel and the binding sites [26], the difference between binding constants is reasonably taken as arising from ion-ion repulsion. With binding constants of 70 M^{-1} and 1 M^{-1}, for the malonyl dimer, this means a free energy of repulsion of 2.5 kcal/mole at a distance of 21 Å [17, 26]. Since the barrier for entry of the second ion is only a few angstroms further away than the occupied binding site, say at 23 Å, a similar repulsion is expected at this distance and the on-rate constant for the second ion would be expected to be one to two orders of magnitude smaller than the on-rate constant for the first ion. Both sodium-23 nuclear magnetic resonance determined rate constants [31, 32] and earlier fittings to single-channel conductances using a two-site model [15], however, showed the on-rate constants for the first and second ion to be of similar magnitude. This apparent paradox has been explained by the first ion jumping back and forth between both halves of the channel faster than either half of the channel can relax to the conformation of the unoccupied channel [30]; that is, the first ion holds the channel in a librated state favorable for ion interaction such that the carbonyls at the mouth are already partially librated inward for entry of the second ion. In this regard, it is helpful to realize that the outermost carbonyls at the mouth are part of the binding site [26]. With slightly more than 10^7 sodium ions/sec passing through the channel for conditions of 1 M NaCl, 100 mV applied potential and 25°C, and with estimates of the rate constant for jumping over the central barrier of the order of 10^7 sec^{-1} [13, 15] and of the on-rate constants of 10^7 sec^{-1}, this requires that the rate

constant for relaxation from the metastable state must be slower than 10^7 sec^{-1}. It cannot be a great deal slower otherwise it would simply be part of the turning-on process of the channel and the on-rate constant for the first ion would again be faster. This same analysis applies with the rate constants recently reported by Eisenman and Sandblom (9) for glyceryl monooleate bilayers where an additional pair of outer sites, external to the barrier at the channel mouth, are included; and in an analogous manner these authors spoke of conformational stabilization to relax expected ion-ion repulsions. The perspective is that the relaxation process is fast enough to occur during the period that the channel is empty but sufficiently slow during single-channel occupancy such that the single ion can hold both monomers comprising the dimeric channel in the metastable state.

A proposed mechanism whereby these metastable states might exist involves the effects of side chain orientations and interactions on the energetics of libration [30]. An elemental libration for a stable helical state such as an α-helix can be thought of as a rapid process with a time constant in the picosecond range and it would exhibit relatively small excursions from the equilibrium position. The repeating unit in the $\beta^{6,3}_{3,3}$-helix, however, is a dipeptide with the C-O moieties pointing in alternate directions approximately parallel and antiparallel to the helix axis, and the β-helix occurs with values of the torsion angles ϕ and ψ, which place it in a region of the ϕ, ψ torsion angle plot where changes in potential energy are small with changes in torsion angles [20, 22, 24, 25, 34]. Furthermore, it appears that there are significant differences in the L- and D-residue carbonyls in terms of interactions with permeant cations. On binding a cation, the carbon-13 nuclear magnetic resonance signal of a carbonyl moiety shifts to lower fields due to the deshielding effect resulting from the electron withdrawing capacity of the cation. Indeed this was the basis for mapping the ion binding sites in the gramicidin A transmembrane channel using carbon-13 enriched L-residue carbonyl carbons [22, 26]. It has been found, however, for the D-residue carbonyls in the region of the cation binding site that these carbonyl carbon resonances shift slightly upfield on ion binding [29, 33]. This implies that the carbonyls of the D-residues tilt outward toward the lipid, an interpretation supported by conformational energy calculations [34]. Thus the librational motion of the β-helices appears more complicated and would involve the inward libration of the L-carbonyl moieties coupled to the outward libration of the D-carbonyl moieties. This peptide libration mechanism then would be a slower process (reasonably in the microsecond range) and importantly can be significantly affected by side chain orientations and by the interactions between side chains, particularly the interactions between side chains of residues i and $i + 1$ and residues i and $i + 6$ as previously noted [30].

In this report, the consideration of metastable, librated conducting states is introduced in connection with nonlinearity of the ln (single channel conductance) *versus* inverse temperature plots and data are presented for the temperature dependence of the most probable potassium single channel currents in gramicidin A-doped black lipid membranes comprised of diphytanoyl phosphatidylcholine/*n*-decane.

Materials and Methods

Black lipid membranes were formed as previously described [5, 6], on a 0.6-mm diameter aperture separating two Teflon chambers, each filled with 7 ml of 1 M KCl solution. The lipid solution used to form the membrane consisted of 2% (wt/vol) diphytanoyllecithin (DPhL) in *n*-decane. Picomolar concentrations of HPLC purified ^{13}C Val_1 GA [28] were added to the bath from methanolic stock solutions. The temperature was maintained within ± 0.1°C by means of a Peltier cell sandwiched to the bottom of an aluminum block containing the cell and surrounded by styrofoam. Temperature of the cell was controlled by a power supply built in this laboratory and two Peltier thermoelectric modules, cat. no. CP1.4-35-06L and CP1.4-71-06L from MELCOR, Trenton, N.J. The power supply contains a 5 Ampere Hour rechargeable battery and a current controlled charging circuit. The current control circuit also serves as temperature set and control for current from the battery to the Peltier cells. The experiments were carried out for various temperatures in the range of 15 to 47°C, and three separate temperature studies have been carried out. The temperature was monitored by means of a 29-gauge thermocouple inserted into a hole (drilled in the partition) that reaches from the top of the partition to a point at the same level of but 5 mm from the planar bilayer. The voltage was applied to the membrane from a battery-operated voltage source through Ag-AgCl electrodes.

The membrane cell is completely contained in a closed metal box which acts as an electric shield. The metal box was placed on a round concrete slab, which was mounted on an inflated automobile innertube. The entire set up was placed on top of a vibration-free table (MICRO-g series 61) for further shielding from mechanical vibrations.

The block diagram of the set-up used for recording single-channel events is shown in Fig. 2. The membrane potential was clamped at 100 mV. The output signal of the cell membrane was delivered to a Keithley 427 current amplifier, which, in the case of GA, was set with a rise time lying in the range 0.03 to 30 msec. The output signal of the amplifier was passed through a Krohn-Hite filter model 3342. This is a two-channel filter that can function as a high-pass or a low-pass filter with an attenuation rate of 96 db per octave. It has digitally tuned cutoff frequencies over the range from 0.001 Hz to 99.9 kHz. In the present set of experiments, the low pass RC mode was used in the range 25–100 Hz.

In order to obtain the single-channel conductance fluctua-

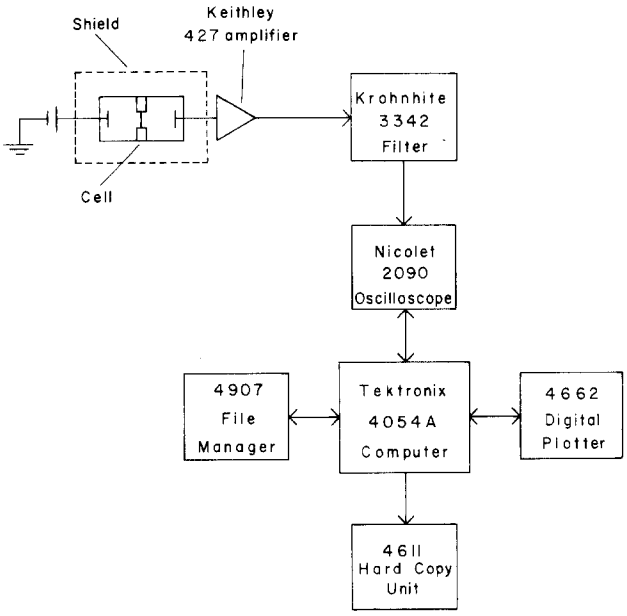

Fig. 2. Block diagram of the experimental set-up for the single-channel measurements. The cell, contained in a box for better shielding, with the current/amplifier is mounted on a vibration free table. The signal coming from the cell is amplified, filtered, recorded, and analyzed by the computer. Permanent records can be obtained from the computer, the digital plotter, and the hard copy unit

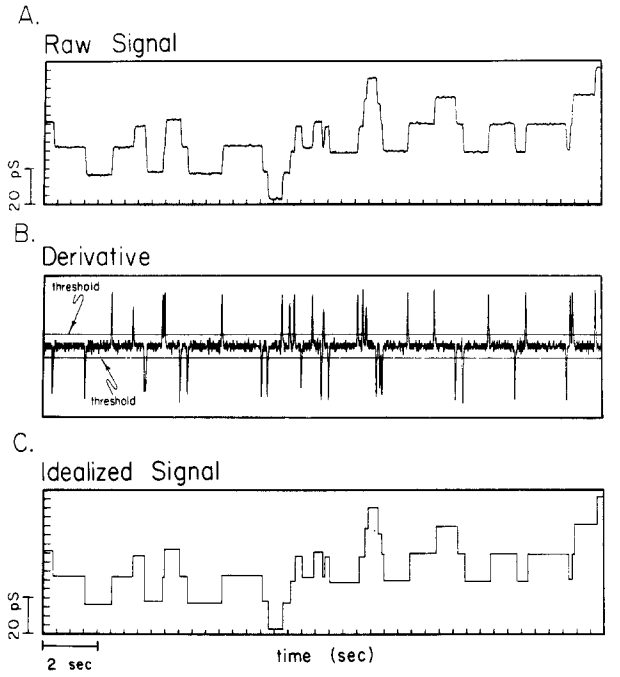

Fig. 3. The scheme for the recognition of single-channel transitions. (*A*): The raw signal composed of 4096 points spanning a time window of 20.48 sec. (*B*): The derivative of the signal. Note that the peaks surpassing the threshold level correspond to transitions in *A*. (*C*): The idealized signal reconstructed by the algorithm showing the essential features of *A*

tion data in a digital form suitable for later analysis in a computer, the output stage of the filter was connected to a Nicolet Explorer III Model 2090 digital oscilloscope with a built-in floppy disk drive. This enabled eight sweeps of voltage fluctuations to be recorded in a single $5\frac{1}{4}''$ diskette with each sweep consisting of 4096 data points (voltage values). The sampling time interval was determined by a switch setting on the oscilloscope.

The analysis of the single-channel conductance data was performed on a Tektronix 4054A graphic computing system with 54K of main memory and supported by two Tektronix signal processing ROM packs. The Tektronix computer was connected to the Nicolet oscilloscope through an RS-232 interface operating at 9600 baud rate. This allows the data stored in the Nicolet floppy diskettes to be brought into the computer. The routines for analyzing the data were written in enhanced BASIC language.

Figure 3 shows the method employed to delineate "jumps" in voltage. The "jump" recognition is based on a rapid evaluation of the derivative of the raw signal. The regions where the absolute value of the derivative exceeds a chosen "threshold" value, δ, are identified (Fig. 3*B*). If δ is properly set, these regions are where jumps occur in the raw signal. Mean conductance levels before and after a transition are obtained by averaging the raw signal excluding the regions where transitions are encountered. The resulting "idealized" signal seen in Fig. 3*C* clearly shows all the relevant channel events. While the original signal requires 4096 data points, the idealized signal can be described by $2n$ data points where n is the total number of channel jumps in the given sweep and therefore requires much reduced disk space in the computer. The entire analysis takes about 50 sec per sweep of 4096 data points in the Tektronix computer. Both the evaluation of the derivative of the signal and the calculation of the time points where the derivative "crosses" the selected threshold δ are performed utilizing two powerful routines "DIF3" and "CROSS" microprogrammed in the Tektronix signal processing ROM pack No. 1.

The method of analysis of the channel events to obtain estimates of single-channel conductances and the single-channel lifetimes depends on the complexity of the channel events in each sweep. The algorithmic efforts required have been elegantly discussed recently by Horn and Lange [16]. To facilitate description of the various approaches employed here, several hypothetical conductance traces are shown in Fig. 4. The simplest case is, of course, when all the events recorded *appear* to be at the single-channel level with a clear delineation of the base-line, as in Fig. 4*A*. Two channel events are seen here, one with a conductance h_1 and a lifetime of t_2-t_1 and another for a duration of t_4-t_3 with a conductance h_2. Once the raw signals are idealized as in Fig. 3 by recognizing the times and heights of the various jumps, it is a straightforward matter to estimate in the computer the conductance and the lifetime of each complete single-channel event for such simple traces. As long as only one channel is open at a given time, the proper matching of "down" jump with the corresponding "up" jump can always be ensured, even if several channels of identical heights are seen in a given sweep.

When more than one channel remains open at a given time, a unique identification of channel lifetimes is not always possible. However, if channel heights are different (i.e., differing by more than the RMS error in conductance estimation) unambiguous identification is possible. Thus, in Fig. 4*B*, the down jump at

t_3 is readily matched with the up jump at t_1, and jumps at t_2 and at t_4 must correspond to each other. Similarly, the jumps at t_7 and t_8 must be matched, respectively, to the jumps at t_6 and t_5. There is a question of interpretation that arises even when the jumps are properly matched for multiple events of the type shown occurring between t_5 and t_8 in Fig. 4*B*. This has to do with whether the two channel jumps seen at t_5 and t_6 pertain to two different conducting states of a given molecule or to "opening" of two different channel molecules. We have assumed the later interpretation in this work. (Note that such an ambiguity does not arise with the first set of multiple events occurring between t_1 and t_4.) This assumption must be borne in mind when interpreting the conductance histograms. If they are taken to be two different states of the same molecule, then the conductances would have been h_1 and $h_1 + h_2$. Instead, we assume that these are the conducting states of two different molecules and therefore h_1 and h_2 are taken to be the conductances.

Difficulties arise when several channel jumps of identical heights are encountered as shown in Fig. 4*C*. Does the down transition at t_3 correspond to the opening at t_1 or the one at t_2? A proper resolution of this ambiguity is needed for an accurate determination of lifetimes. The method employed in this article for properly matching the downward transitions with their respective upward transitions may be described by the following algorithm: each sweep is analyzed from left to right. As an upward jump is encountered, it is stored in a buffer array. When a downward jump is detected, the buffer array is searched, starting from the most recent upward jump and going backward in time, for an upward transition with the height closest to the given downward transition. Having chosen the best match, the difference in height between the jumps is computed. If this difference is less than a chosen tolerance limit, then the jumps are considered to be matched; the upward transition is removed from the buffer. The lifetime of the channel event is computed. If the difference is greater than the tolerance, the match is discarded and the downward jump is ignored. The tolerance employed depends on the rms value of the base-line noise. A value of 1 pS is found to work satisfactorily with the data presented here.

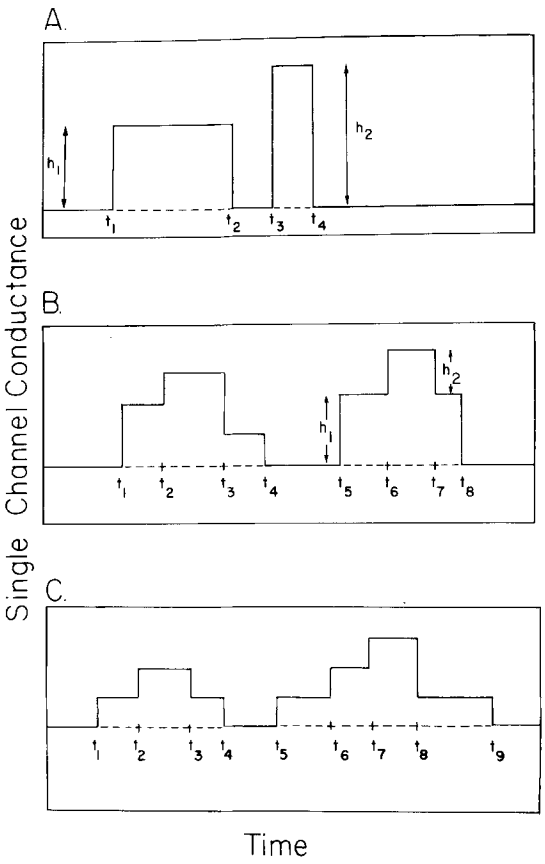

Fig. 4. Hypothetical single-channel transitions (*see* text for discussion)

Results

The single-channel histograms obtained using the various algorithms (i.e., counting upward transitions, downward transitions and by employing the ← algorithm to properly match the downward transitions with their respective upward transitions) are given in Figs. 5 and 6 for various temperatures. A tolerance of 1 pS was employed for the algorithm and the conductance bin width is 0.25 pS. The conductance of the dominant peak remains essentially the same for all the three algorithms. This is the case for each temperature. Figure 5*A* and *B* shows a small peak at ~30 pS due to transitions encountered corresponding to almost "simultaneous" opening or closing of two channels. However, in Fig. 5*C*, the peak at 30 pS is much reduced since the chances of simultaneously opening *and* closing of more than one channel is rather low.

In Fig. 5, in addition to the single-channel histograms, the single channel events have been completely depicted for 15.5°C as a density plot in a conductance-lifetime plane (Fig. 5*D*) and also as a three-dimensional stereo plot showing the frequency of occurrence against conductance and lifetime (Fig. 5*E*). Lifetime histograms can be readily computed from the list of single channel events compiled. Interestingly, one may also obtain lifetime histograms for events corresponding to various conductance states. Thus, by utilizing the conductance histograms, one may pick any desired range of conductance values and compute a lifetime histogram for that range of conductance. This approach is illustrated in Fig. 5*F* where, for 15.5°C, the lifetime histogram for all states seen in Fig. 5*C* is plotted. The inset of Fig. 5*F* displays the natural logarithm of the lifetime probability against channel lifetime. From the slope of the initial linear part of that plot, a mean lifetime of 1.54 sec is estimated. The 27 points, used in the inset of Fig. 5*F* to obtain the mean lifetime, represent 60% of the events being considered.

An additional point that derives from the single channel event analyses is an upper limit approxima-

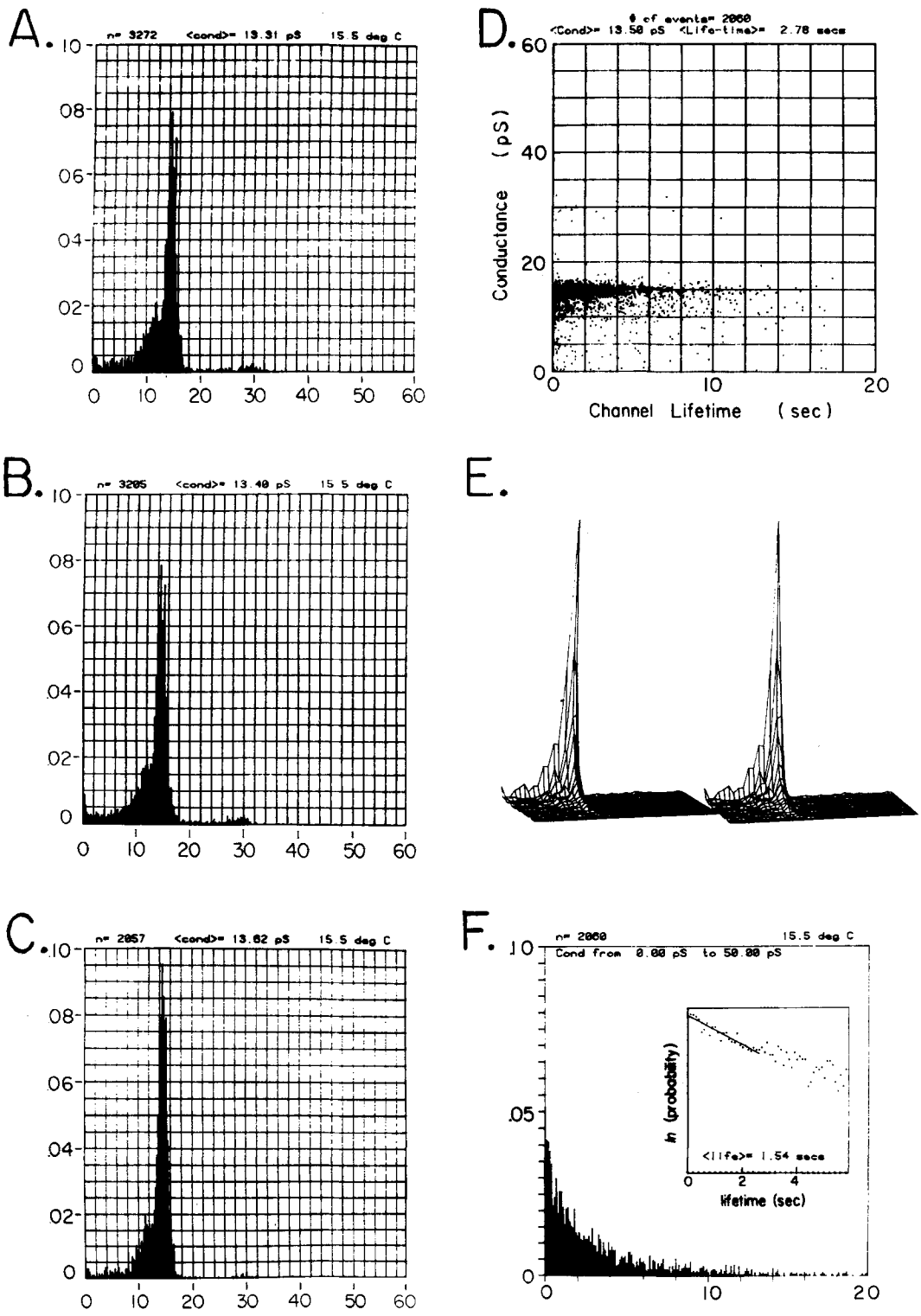

Fig. 5. Single-channel conductance histogram for gramicidin A in DPhL membranes at 15.5°C (*A-C*). *A* is obtained by considering only upward transitions, while *B* is obtained with downward transitions. *C* corresponds to the single-channel events recognized by the "backward" matching algorithm. In each case, the total number of events, *n*, included in the counting and the resulting mean single-channel conductance over all conducting state seen in the histogram are marked. Also, *D* shows a two-dimensional density plot in the conductance-lifetime plane depicting the single channel events captured by the algorithm. The same information is shown in *E* as a three-dimensional histogram in stereo of frequency of occurrence (height) plotted against conductance and lifetime. *F* is the lifetime histogram for all conducting states. The inset in *F* displays the ln (probability) against channel lifetime illustrating the computations of the mean lifetime to be 1.54 sec from the slope of the linear plot at short times

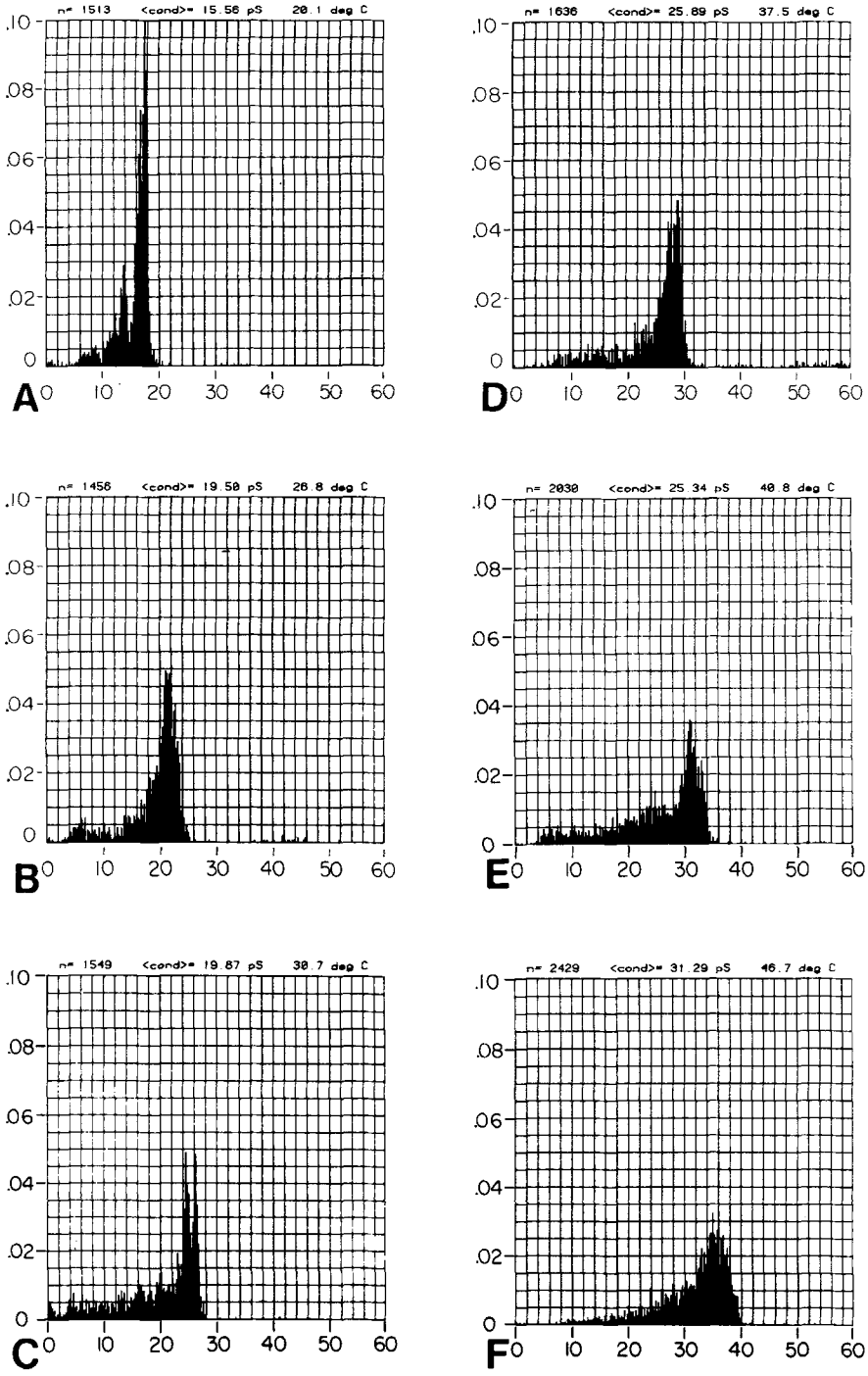

Fig. 6. Same as Fig. 5*C* except at different temperatures: *A*, 20.1°C; *B*, 26.8°C; *C*, 30.7°C; *D*, 36.7°C; *E*, 40.8°C; and *F*, 46.9°C

tion to the probability or rate of transition between conducting states. At all temperatures with the exception of the 37.5°C data, it is seen that there are about 65% of the states retained when there is a matching of a downward transition with a preceding upward transition. This places a maximum probability of about 0.35 for a conducting channel to undergo a change in conductance state. Taking the mean lifetime for all conductance states at 15.5°C to be 1.54 sec (*see* inset of Fig. 5*F*) gives a mean lifetime for conversion between conducting states of about 4.4 sec or a rate of conversion of about 0.23/sec. Such considerations can, of course, be more finely defined in terms of identifiable conductance windows. The conditions for the collection of the 37.5°C data were chosen to demonstrate a caveat in

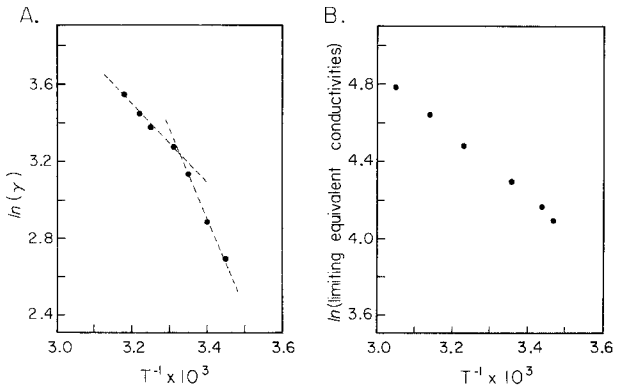

Fig. 7. (*A*): Plot of ln (conductance in picoSiemens) as a function of the reciprocal temperature for GA in diphytanoyl lecithin/*n*-decane at 100 mV membrane voltage and 1 M KCl. (*B*): Plot of ln (limiting equivalent conductivities) as a function of the reciprocal temperature for KCl in water, as calculated from Robinson and Stokes (1955, Appendix Table 6.2 [22*a*]). Note that the limiting high temperature slopes are essentially the same but that the low temperature slope for GA channel transport is much steeper. This means that at high temperature channel transport is diffusion limited while at lower temperatures passage through the channel is rate limiting. The question is by what mechanism does the barrier to transport through the channel decrease with increasing temperature. Both temperature-dependent distribution of helically librated states of the channel and of lipid membrane viscosity are considered. The viscosity effect is proposed to couple ion movements through the channel by means of effects of side-chain motion on energetics of peptide libration required for ion coordination

the analysis of single-channel conductance data relative to the probability of a change in conductance state. When there are a larger number of channel events occurring simultaneously such that analysis windows begin and/or end with several channels on (i.e., unmatched with their "on" or "off" transition), then the foregoing considerations of conductance-state changes during a channel lifetime do not obtain.

Throughout the temperature studies, the histograms of the single-channel conductances demonstrate a well-defined set of most probable conductance states. The less probable states seem to have groupings at some temperatures, but there is not an entirely consistent and obvious shift of these states with temperature. It may be that a proper consideration of these states will require a larger number of events to improve the statistics. There is also a question at 30.7°C in Fig. 6*C* as to whether the most probable conducting state can be separated into two discernible states. For our concerns here, however, this potential finer delineation will not be pursued. A rather broader consideration is followed, recognizing that the potential two states at higher conductances in Fig. 6*C* fall within the conductance window width of the other most probable states. At all temperatures, there is a set of most probable conductance states that fall with a reasonably well-defined Gaussian-like distribution at the upper boundary of the conductance histogram. Since this collection of states remains so readily identifiable, it is reasonable and appropriate to consider the temperature dependence of conductance for this dominant set of conductance states. This is done in the following Discussion.

Discussion

A plot of the natural logarithm of the single-channel conductance in picoSiemens as a function of inverse temperature is given in Fig. 7*A* over the temperature range of 15 to 47°C. What is apparent is that the plot is systematically nonlinear. This nonlinearity has been obtained in three different titrations and indicates that the conductance process cannot be treated as a simple rate process to be fit by the Arrhenius equation, i.e.,

$$\gamma = Ce^{-E_{\exp}/RT} \tag{1}$$

and

$$\ln \gamma = \ln C - E_{\exp}/RT \tag{2}$$

nor as a simple rate process expressed in terms of the Eyring rate equation, i.e.,

$$\gamma = Ck' = C\frac{kT}{h}e^{-\Delta G\ddagger/RT} \tag{3}$$

$$\gamma = Ck' = C\frac{kT}{h}e^{\Delta S\ddagger/R}e^{-\Delta H\ddagger/RT} \tag{4}$$

and

$$\ln \gamma = \ln C' + \ln T + \frac{\Delta S\ddagger}{R} - \frac{\Delta H\ddagger}{RT}. \tag{5}$$

As the effect of ln T is to give only a slight upward curvature, the curve in either case should be essentially linear with the slope equal to $-E_{\exp}/R$ or to $-\Delta H\ddagger/R$.

Several sources of the nonlinearity might be considered: (i) the presence of a series of controlling barriers instead of a single rate-limiting barrier, (ii) the dynamic nature of the channel wherein the distribution of channel states has an intrinsic temperature dependence, and (iii) a temperature dependence of the dynamic channel wherein the viscous drag of the lipid affecting side chain motions is a

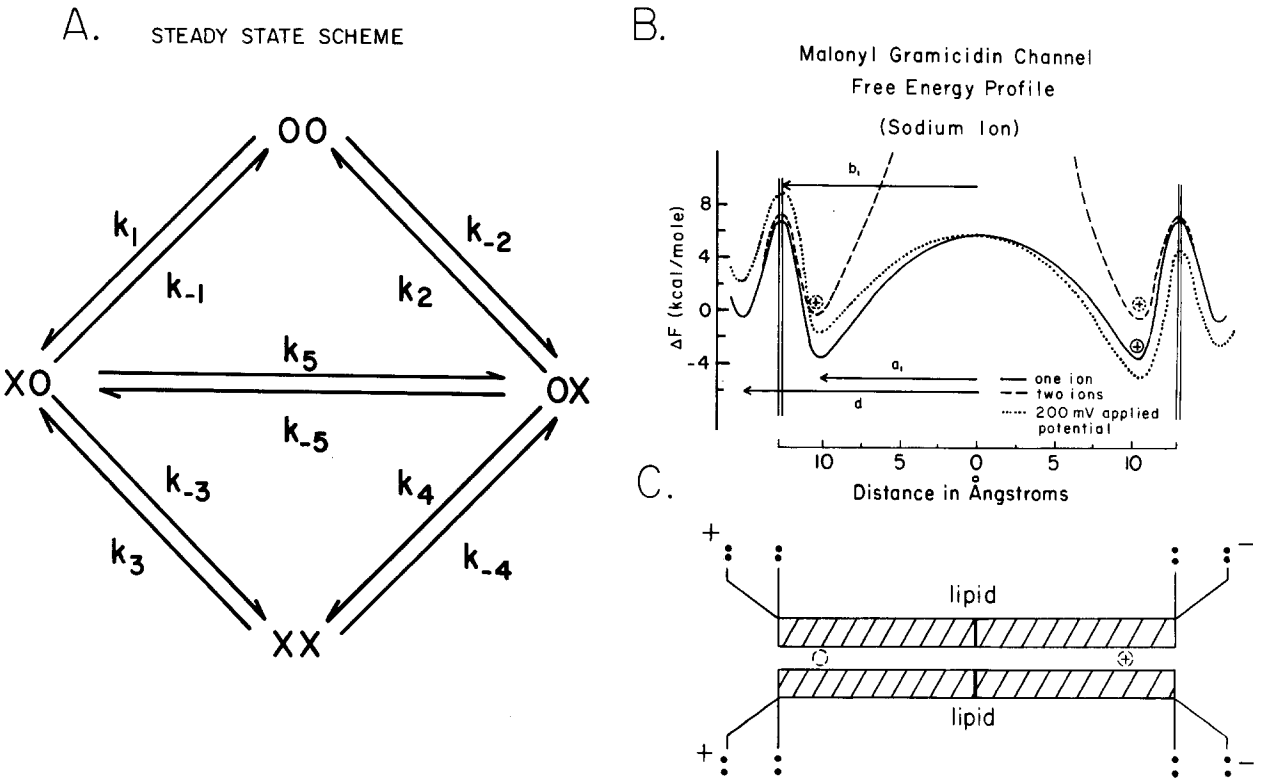

Fig. 8. Two-site mechanism for transport through the gramicidin A channel. (*A*): Steady-state scheme defining the individual rate constants. (*B*): Free energy profile defining relevant lengths and barriers. (*C*): Schematic of channel spanning a membrane, aligned with part *B*. (Reproduced with permission from ref. 32)

dominant factor. The general expression for single channel conductance, γ, can be written

$$\gamma = \frac{i}{V} = \frac{ze}{V} \sum_r \chi_r \sum_s \lambda_{rs} q_{rs} \tag{6}$$

where i, V, z and e are the single-channel current, the transmembrane potential, the charge on the ion, and the coulombs per unit charge, i.e., 1.6×10^{-19} C, respectively. The χ_r are the probabilities of the states of the channel, i.e., for a two binding site channel, $\chi(oo)$ would be the probability of the empty channel, $\chi(ox)$ and $\chi(xo)$ the probabilities for single occupancy and $\chi(xx)$ the probability for two ions in the channel [31]. Each elemental ionic jump begins in state r and ends in state s. Starting with the ion in a particular state r, the summation over s is the listing of the rate processes available to the ion which in a single filing channel are no more than two: to go forward or backward. The q_{rs} are the rate processes for movements of ions within the channel and leaving the channel wherein q_{rs} is simply the specific rate constant and the rate processes for movements of ions into the channel wherein q_{rs} is the product of the ion activity times the specific rate constant. The quantity, λ_{rs}, is the fractional length of the ion movement through the channel and is a signed quantity being positive for movement along the field and negative against the field.

The effect of multiple barriers on the linearity of the temperature dependence can be directly assessed using the single-channel current expression which has been shown to be effective in calculating the single-channel currents using experimentally derived binding and rate constants and to do so over wide ranges of ion activity and transmembrane potential [31]. The scheme for a two-site model is given in Fig. 8 and the two-site current equation can be written [31, 32] as

$$\begin{aligned} i = (ze/2d)\{&(d - a_1)(C'_x k_1 - C''_x k_{-2})\chi(oo) \\ &+ [2a_1 k_5 - (d - a_1)(k_{-1} + C''_x k_{-3})]\chi(xo) \\ &+ [(d - a_1)(k_2 + C'_x k_4) - 2a_1 k_{-5}]\chi(ox) \\ &+ (d - a_1)(k_3 - k_{-4})\chi(xx)\} \end{aligned} \tag{7}$$

where the k_i are defined in Fig. 8*A*, the subscript x stands for the ionic species, the concentrations of which, C'_x and C''_x, are for each of the two sides of the membrane. The lengths a_1, b_1 and d are defined

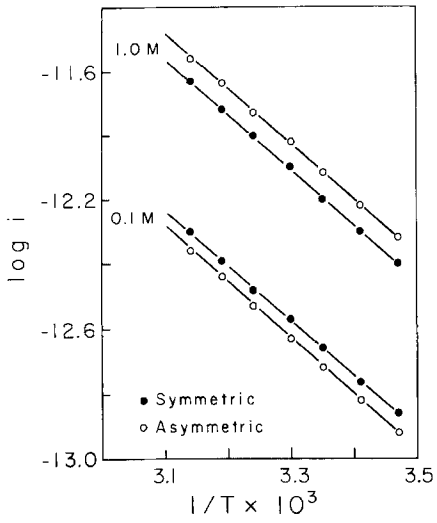

Fig. 9. Calculated temperature dependence of transport using Eq. (7) and the definitions in Eq. 8 and Fig. 8. Note that a plot of the log (single-channel current) *vs.* reciprocal temperature is linear at both 0.1 and 1 M ion activities (which compares conditions of single occupancy and some double occupancy) and for symmetric (●) as well as asymmetric (○) channels. *See* text for discussion

in Fig. 8*B*. With the rate constants known, for example, for Na^+ transport through the malonyl gramicidin A channel, the $\Delta G_i^{\ddagger}$ can be calculated by Eq. (3). These are listed below with the voltage dependence included with the definitions $l_1 = d - b_1$, $l_2 = b_1 - a_1$ where $d = 15$ Å, $a_1 = 10.5$ Å and $b_1 = 13$ Å. Defining $\phi = zFV/2dRT$ with F = the Faraday constant

$$\begin{aligned}
\Delta G_1^{\ddagger} &= 7.25 + l_1\phi & \Delta G_{-1}^{\ddagger} &= 9.98 - l_2\phi \\
\Delta G_2^{\ddagger} &= 9.98 + l_2\phi & \Delta G_{-2}^{\ddagger} &= 7.25 - l_1\phi \\
\Delta G_3^{\ddagger} &= 7.49 + l_2\phi & \Delta G_{-3}^{\ddagger} &= 7.49 - l_1\phi \\
\Delta G_4^{\ddagger} &= 7.49 + l_1\phi & \Delta G_{-4}^{\ddagger} &= 7.49 - l_2\phi \\
\Delta G_5^{\ddagger} &= 8.57 + a_1\phi & \Delta G_{-5}^{\ddagger} &= 8.57 - a_1\phi. \qquad (8)
\end{aligned}$$

Taking the $\Delta S_i^{\ddagger}$ to be zero, i.e., $\Delta G_i^{\ddagger} = \Delta H_i^{\ddagger}$, it is possible to assess the sole effect of multiple barriers on linearity of log (current or conductance) *vs.* reciprocal temperature. This is shown in Fig. 9 where the plots are seen to be linear for both molal activities of 1.0 and 0.1. Similarly by raising the *ox* state and the right-hand barrier of Fig. 8*B* by one kcal/mole to give an asymmetric channel, the plot is yet linear. It seems that multiple barriers of this sort do not give rise to significant nonlinearity. This small change does give rise to very asymmetric *I/V* curves [23] similar to those observed by Busath and Szabo [7].

Of course, the $\Delta S_i^{\ddagger}$ are not zero and neither are they necessarily of equivalent magnitude for each barrier. In particular, it is intuitively expected that the $\Delta S_i^{\ddagger}$ will be greater for the two entrance-exit barriers than for the central barrier. This effect has been suggested by H. Frauenfelder as a possible source of nonlinearity of the log *i vs.* T^{-1} plot (*private communication*). Sodium-23 NMR data is presently being analyzed to determine the ΔS for binding to the channel for both single and double occupancy over the temperature range of 15 to 70°C. These results and evaluation of the entropy of activation for the central barrier and for the ions leaving the channel should provide the information required to evaluate this possibility. As the central barrier is higher for the malonyl dimer, if this effect is significant, it might be expected that log *i vs.* T^{-1} would be more nonlinear for the malonyl dimer of gramicidin A than for gramicidin A itself. This is because, as the temperature is raised, the central barrier would become a more significant factor in determining the net current for the malonyl gramicidin A channel.

The dynamic nature of the channel may now be considered for the nonlinearity seen in Fig. 7*A*. In the Introduction arguments were presented for the presence of conformational states being selected by the ion but these states are metastable for the unoccupied channel. Therefore for a given ion, two distributions of channel states may be considered: Ch_o, the preferred distribution of conformational states in the absence of ion, and Ch_l, a selected peptide librated, conformational state that occurs on occupancy. If P_o and P_l are the probabilities of the two states, then the ratio

$$K^{\circ} = \frac{P_o}{P_l} \qquad (9)$$

is the equilibrium constant for the interconversion

$$Ch_o \rightleftarrows Ch_l. \qquad (10)$$

Since $P_o + P_l = 1$ and by Eq. (9) $P_o = K^{\circ}P_l$, then the probability or the fraction of the time, P_l, that the channel is in the librated state becomes

$$P_l = 1/(1 + K^{\circ}). \qquad (11)$$

If the librated state (or states when considering different side-chain orientations, for example) is considered to be the conducting state and Ch_o to be a nonconducting or relatively poorly conducting collection of states, Eq. (6) should be divided by $1 + K$ in order to correct for the temperature dependence of the changing fraction of time that a channel is in

an appropriately librated state. This gives for the complete expression

$$i_x = ze \sum_r \chi_r \sum_s \lambda_{rs} q_{rs} (1 + \bar{K}^\circ_{rs})^{-1}. \tag{12}$$

Taking $\bar{\Delta}S^\ddagger$ and $\bar{\Delta}H^\ddagger$ to be the mean entropy and enthalpy, responsible for the rate-limiting process of conductance, considering an average equilibrium constant, $\bar{K}^\circ$, and since

$$\bar{K}^\circ = e^{-\overline{\Delta G}^\circ/RT} = e^{\overline{\Delta S}^\circ/R} e^{-\overline{\Delta H}^\circ/RT} \tag{13}$$

then

$$\ln \gamma = \ln C' + \ln T + \frac{\bar{\Delta}S^\ddagger}{R} - \frac{\bar{\Delta}H^\ddagger}{RT} - \ln(1 + e^{\overline{\Delta S}^\circ/R}\, e^{-\overline{\Delta H}^\circ/RT}). \tag{14}$$

At low temperatures, the probability of the librated state is lower and $P_o > P_l$. As the temperature increases P_l approaches P_o in magnitude and K° approaches one. Also it appears from the data in Fig. 7*A* that a limiting slope is being approached at high temperatures and that the limiting slope is quite low, approaching the range for a diffusion controlled process.

Taking for the diffusion controlled limit a value of 3.5 kcal/mole for $\overline{\Delta H}^\ddagger$, $\overline{\Delta S}^\circ$ and $\overline{\Delta H}^\circ$ can be estimated by obtaining a fit to the curve. The values used to approximate the curve of Fig. 7*A* are a $\overline{\Delta S}^\circ$ of -15 cal/mole degree and a $\overline{\Delta H}^\circ$ of -5 kcal/mole channels. While these values introduce curvature of the correct sign, Eq. (14) as given is unable to reproduce the dramatic nonlinearity that is experimentally observed and the significance of the quantities is not immediately apparent.

The approximations of Eq. (14) have taken K^+ transport to be a mean rate process and have considered an average conformational equilbrium represented by $\bar{K}^\circ$. In reality, of course, for each elemental rate process in Eq. (7) and represented in Fig. 8 as k_i, there are a number of side-chain orientations possible, each of which would give rise to different librational energetics with its associated K. Accordingly, the process is considerably more complex than represented by Eq. (14). Nonetheless, the point is made that the channel is a dynamic structure and the present effort can be taken as an explicit example of the kinetic properties of channels which have been considered in more general terms by Läuger [19].

Another approach may be considered for treating a dynamic channel, an approach which recognizes the surrounding viscous lipid layer of the membrane. It has been argued that side-chain orientation can affect the energetics of peptide carbonyl libration required for lateral coordination of the ion. The rate of side-chain reorientation even within a local minimum depends on the viscosity of the lipid. Conceivably, even different locations within the oscillations of a localized side-chain minimum could give rise to different peptide librational energetics. Thus Eq. (5) may be rewritten

$$\ln \gamma = \ln C' + \ln T + \frac{\delta S^\ddagger(\eta)}{R} - \frac{\delta H^\ddagger(\eta)}{RT} \tag{15}$$

where $\delta S^\ddagger(\eta)$ and $\delta H^\ddagger(\eta)$ explicitly note that these quantities are a function of the viscosity, η, of the lipid. A similar viscosity dependence has been considered by Debrunner and Frauenfelder in studies of ligand binding to myoglobin and hemoglobin [8]. As the viscosity of the lipid is a function of temperature, in this formalism $\delta S^\ddagger(\eta)$ and $\delta H^\ddagger(\eta)$ change with temperature. Accordingly, an analytical approach can be used which divides the temperature study into a set of segments, i, each with its own $\delta S^\ddagger_i$ and $\delta H^\ddagger_i$. This is done by fitting a smoothed curve to the data and taking tangents to the curve at various temperatures. From the tangents are calculated the $\delta H^\ddagger$ at that temperature and the plot of the ln $\delta H^\ddagger$ *versus* T^{-1} gives a new enthalpy which would, in our perspective, involve the energy for side-chain redistribution in the presence of a particular lipid. While determination of conductance states within a lipid membrane below the liquid-crystalline to gel phase transition would provide an interesting boundary condition, an evaluation of the single-channel currents below the transition temperature of the lipid is made difficult by the absence of the on-off process, which allows measurement of the single-channel current magnitudes. That conductance continues below the lipid transition temperature was early shown by Krasne et al. [18] in terms of macroscopic conductance.

A complete description of gramicidin channel conductance is undoubtedly going to be complex [12]. As a model system, however, it is ideal for approaching these complicating factors of transport reaction kinetics because of its relatively simple structure and because of the relative ease of obtaining chemical modifications and analogues. The emerging perspective, however, should not be lost in the increasing complexity. The peptide moieties of the channel librate to form the conducting channel, and when appropriately librated at elevated temperatures the barriers for entering and passing through the channel are so low for 1 M KCl that the rate-limiting process is diffusion to the mouth of the

channel. The proposal that conductance can be diffusion limited has already been put forward by Andersen and Procopio [1]. With the rate-limiting barrier being at the mouth of the channel, at lower temperatures the magnitude of the barrier is a combination of the barrier for partial dehydration-hydration plus a complicated energy component due to peptide libration. Although the rate-limiting barrier appears to be at the mouth of the channel in phosphatidyl choline membranes, this may not be the case for membranes made from straight-chain monoglycerides (10). Since the peptide libration energetics can be expected to be lipid dependent principally by means of the dependence of side-chain orientation on lipid and the dependence of peptide libration energetics on side-chain orientation, it is reasonable to expect that the temperature at which conductance becomes diffusion limited would vary with membrane lipid. The marked degree of nonlinearity observed in Fig. 7*A* may be due to the branched chain phytanoyl moiety, which could more effectively (due to a greater viscous drag) dampen side-chain reorientation necessary to facilitate libration. Additionally, of course, the energetics for peptide libration should also be different for permeable monovalent cations of different ionic radii and would, as originally suggested [24, 25] be a basis for monovalent cation selectivity. Future studies will examine the lipid and the ion dependence of the nonlinearity.

This work was supported in part by the National Institutes of Health, Grant No. GM-26898. The authors wish to thank K. U. Prasad for preparing the sample of synthetic gramicidin A, and P. Läuger for the gift of the membrane cells.

References

1. Anderson, O.S., Procopio, J. 1980. Ion movements through gramicidin A channels. On the importance of the aqueous diffusion resistance and ion water interactions. *Acta Physiol. Scand. Suppl.* **481**:27–35
2. Apell, H.-J., Bamberg, E., Alpes, H., Läuger, P. 1977. Formation of ion channels by a negatively charged analog of gramicidin A. *J. Membrane Biol.* **31**:171–188
3. Bamberg, E., Apell, H.-J., Alpes, H. 1977. Structure of the gramicidin A channel: Discrimination between the L,D, and the πL,D helix by electrical measurements with lipid bilayer membranes. *Proc. Natl. Acad. Sci. USA* **74**:2402–2406
4. Bamberg, E., Noda, K., Gross, E., Läuger, P. 1976. Single-channel parameters of gramicidin A, B and C. *Biochim. Biophys. Acta* **419**:223–228
5. Bradley, R.J., Romine, W.O., Long, M.M., Ohnishi, T., Jacobs, M.A., Urry, D.W. 1977. Synthetic peptide K^+ carrier with Ca^{2+} inhibition. *Arch. Biochem. Biophys.* **178**:468–474
6. Bradley, R.J., Urry, D.W., Okamoto, K., Rapaka, R.S. 1978. Channel structures of gramicidin: Characterization of succinyl derivatives. *Science* **200**:435–437
7. Busath, D., Szabo, G. 1981. Gramicidin forms multi-state rectifying channels. *Nature (London)* **294**:371–373
8. Debrunner, P.G., Frauenfelder, H. 1982. Dynamics of Proteins. *Annu. Rev. Phys. Chem.* **33**:283–299
9. Eisenman, G., Sandblom, J.P. 1983. Energy barriers in ionic channels: Data for gramicidin A interpreted using a single-file (3B4S″) model having three barriers separating 4 sites. *In:* Physical Chemistry of Transmembrane Ion Motions. G. Spach, editor. pp. 329–348. Elsevier Science, Amsterdam
10. Eisenman, G., Sandblom, J., Hagglund, J. 1983. Electrical behavior of single-filing channels. *In:* Structure and Function of Excitable Cells. D.C. Chang, I. Tasaki, W.J. Adelman, Jr., and H.R. Leuchtag, editors. pp. 383–413. Plenum, New York
11. Eisenman, G., Sandblom, J., Neher, E. 1978. Interactions in cation permeation through the gramicidin channel Cs, Rb, K, Na, Li Tl, H and effects of anion binding. *Biophys. J.* **22**:307–340
12. Finkelstein, A., Andersen, O.S. 1981. The gramicidin A channel: A review of its permeability characteristics with special reference to the single-file aspect of transport. *J. Membrane Biol.* **59**:155–171
13. Henze, R., Neher, E., Trapane, T.L., Urry, D.W. 1982. Dielectric relaxation studies of ionic processes in lysolecithin-packaged gramicidin channels. *J. Membrane Biol.* **64**:233–239
14. Hladky, S.B., Haydon, D.A. 1972. Ion transfer across lipid membranes in the presence of gramicidin A: I. Studies of the unit conductance channel. *Biochim. Biophys. Acta* **274**:294–312
15. Hladky, S.B., Urban, B.W., Haydon, D.A. 1979. Ion movements in pores formed by gramicidin A. *In:* Membrane Transport Processes. C.F. Stevens and R.W. Tsien, editors. Vol. 3, p. 89. Raven Press, New York
16. Horn, R., Lange, K. 1983. Estimating kinetic constants from single channel data. *Biophys. J.* **43**:207–223
17. Koeppe, R.E., II, Hodgson, K.O., Stryer, L. 1978. Helical channels in crystals of gramicidin A and of a cesium-gramicidin A complex: An X-ray diffraction study. *J. Mol. Biol.* **121**:41–54
18. Krasne, S., Eisenman, G., Szabo, G. 1971. Freezing and melting of lipid bilayers and the mode of action of nonactin, valinomycin and gramicidin. *Science* **174**:412–415
19. Läuger, P. 1980. Kinetic properties of ion carriers and channels. *J. Membrane Biol.* **57**:163–178
20. Ooi, T., Scott, R.A., Vanderkooi, G., Scheraga, H.A. 1967. Conformational analysis of macromolecules: IV. Helical structures of poly L-alanine, poly L-valine, poly-β-methyl, L-aspartate, poly γ-methyl-L-glutamate and poly L-tyrosine. *J. Chem. Phys.* **46**:4410–4426
21. Prasad, K.U., Trapane, T.L., Busath, D., Szabo, G., Urry, D.W. 1982. Synthesis and characterization of 1-^{13}C-D · Leu^{12,14} gramicidin A. *Int. J. Pept. Protein Res.* **19**:162–171
22. Ramachandran, G.N., Ramakrishnan, C., Sasisekharan, V. 1963. Stereochemistry of polypeptide chain configurations. *J. Mol. Biol.* **7**:95–99

22*a*. Robinson, R.A., Stokes, R.H. 1955. Electrolyte Solutions. Appendix Table 6.2, p. 452. Academic, New York

23. Urry, D.W. 1973. Polypeptide conformation and biological function: β-helices ($\pi_{L,D}$-helices) as permselective transmembrane channels. *In:* Conformation of Biological Molecules and Polymers—The Jerusalem Symposia on Quantum

Chemistry and Biochemistry. E.D. Bergmann and B. Pullman, editors. pp. 723–736. Israel Academy of Sciences, Jerusalem

24. Urry, D.W. 1984. On the molecular structure of the gramicidin transmembrane channel. *In:* The Enzymes of Biological Membranes. A.N. Martonosi, editor. Plenum, New York (*in press*)
25. Urry, D.W., Goodall, M.C., Glickson, J.D., Mayers, D.F. 1971. The gramicidin A transmembrane channel: Characteristics of head to head dimerized $\pi_{(L,D)}$ helices. *Proc. Natl. Acad. Sci. USA* **68:**1907–1911
26. Urry, D.W., Prasad, K.U., Trapane, T.L. 1982. Location of monovalent cation binding sites in the gramicidin channel. *Proc. Natl. Acad. Sci. USA* **79:**390–394
27. Urry, D.W., Trapane, T.L. and Prasad, K.U. 1983. Is the gramicidin A transmembrane channel single stranded or double stranded helix? A simple unequivocal determination. *Science* **221:**1064–1067
28. Urry, D.W., Trapane, T.L., Romanowski, S., Bradley, R.J., Prasad, K.U. 1983. On the use of synthetic gramicidins in the determination of channel structure and mechanism. *Int. J. Pept. Protein Res.* **21:**16–23
29. Urry, D.W., Trapane, T.L., Walker, J.T., Prasad, K.U. 1982. On the relative membrane permeability of Na^+ and Ca^{2+}: A physical basis for the messenger role of Ca^{2+}. *J. Biol. Chem.* **257:**6659–6661
30. Urry, D.W., Venkatachalam, C.M., Prasad, K.U., Bradley, R.J., Parenti-Castelli, G., Lenaz, G. 1981. Conduction processes of the gramicidin channel. *Int. J. Quant. Chem.: Quant. Biol. Symp.* **8:**385–399
31. Urry, D.W., Venkatachalam, C.M., Spisni, A., Bradley, R.J., Trapane, T.L., Prasad, K.U. 1980. The malonyl gramicidin channel: NMR-derived rate constants and comparison of calculated and experimental single channel currents. *J. Membrane Biol.* **55:**29–51
32. Urry, D.W., Venkatachalam, C.M., Spisni, A., Läuger, P., Khaled, M.A. 1980. Rate theory calculation of gramicidin single channel currents using NMR-derived rate constants. *Proc. Natl. Acad. Sci. USA* **77:**2028–2032
33. Urry, D.W., Walker, J.T., Trapane, T.L. 1982. Ion interactions in (1-^{13}C)D-Val^8 and D-Leu^{14} analogs of gramicidin A, the helix sense of the channel and location of ion binding sites. *J. Membrane Biol.* **69:**225–231
34. Venkatachalam, C.M., Urry, D.W. 1984. Theoretical analysis of gramicidin A transmembrane channel: II. Energetics of helical librational states of the channel. *J. Comput. Chem.* **5:**64–71
35. Weinstein, S., Wallace, B., Blout, E.R., Morrow, J.S., Veatch, W. 1979. Conformation of gramicidin A channel in phospholipid vesicles: A ^{13}C and ^{19}F nuclear magnetic resonance study. *Proc. Natl. Acad. Sci. USA* **76:**4230–4234

Received 16 December 1983; revised 7 May 1984